Biogeosciences Discuss., 12, 6929–6969, 2015
www.biogeosciences-discuss.net/12/6929/2015/
doi:10.5194/bgd-12-6929-2015

Biogeosciences Discussions
Open Access

Two decades of inorganic carbon dynamics along the Western Antarctic Peninsula

C. Hauri[1,2,3], S. C. Doney[4], T. Takahashi[5], M. Erickson[6], G. Jiang[7], and H. W. Ducklow[5]

[1]International Pacific Research Center, SOEST, University of Hawai'i, Honolulu, HI, USA
[2]International Arctic Research Center, University of Alaska Fairbanks, Fairbanks, AK, USA
[3]School of Fisheries and Ocean Sciences, University of Alaska Fairbanks, Fairbanks, AK, USA
[4]Marine Chemistry and Geochemistry Department, Woods Hole Oceanographic Institution, Woods Hole, MA, USA
[5]Lamont-Doherty Earth Observatory, Columbia University, Palisades, NY, USA
[6]Antarctic Support Contractor, Arlington, VA, USA
[7]School of Earth Sciences, University of Melbourne, Melbourne, VIC, Australia

Received: 17 April 2015 – Accepted: 21 April 2015 – Published: 7 May 2015

Correspondence to: C. Hauri (chauri@hawaii.edu)

Published by Copernicus Publications on behalf of the European Geosciences Union.

Abstract

We present 20 years of seawater inorganic carbon measurements collected along the western shelf and slope of the Antarctic Peninsula. Water column observations from summertime cruises and seasonal surface underway pCO_2 measurements provide unique insights into the spatial, seasonal and interannual variability of the dynamic system. The discrete measurements from depths > 2000 m align well with World Ocean Circulation Experiment observations across the time-series and underline the consistency of the data set. Analysis shows large spatial gradients in surface alkalinity and dissolved inorganic carbon content, with a concomitant wide range of Ω_{arag} from values < 1 up to 3.9. This spatial variability was mainly driven by increasing influence of biological productivity towards the southern end of the sampling grid and melt water input along the coast towards the northern end. Large inorganic carbon drawdown through biological production in summer caused high near-shore Ω_{arag} despite glacial and sea-ice melt water input. In support of previous studies, we observed Redfield behavior of regional C / N nutrient utilization, while the C / P (80.5 ± 2.5) and N / P (11.7 ± 0.3) molar ratios were significantly lower than the Redfield elemental stoichiometric values. Seasonal predictions of Ω_{arag} suggest that surface waters remained mostly supersaturated with regard to aragonite throughout the study. However, more than a third of the predictions for winters between 1999 and 2013 resulted in $\Omega_{arag} < 1.3$. Such low levels of Ω_{arag} may have implications for important organisms such as pteropods. Despite large interannual variability, surface pCO_2 measurements indicate a statistically significant increasing trend of up to 23 µatm per decade in fall and spring and a concomitant decreasing pH, pointing towards first signs of ocean acidification in the region. The combination of ongoing ocean acidification and freshwater input may soon provoke more unfavorable conditions than what the ecosystem experiences today.

BGD
12, 6929–6969, 2015

1 Introduction

Antarctic continental shelves are viewed as strong anthropogenic CO_2 sinks and therefore play an important role in global biogeochemical cycles (Arrigo et al., 2008). These highly productive regions also support productive ecosystems that are exposed to rapid environmental changes (Ducklow et al., 2007, 2012). Conditions along the western shelf of the Antarctic Peninsula (WAP, Fig. 1) are characterized by rapid ocean–atmosphere warming, sea-ice retreat and melting of glaciers (Ducklow et al., 2012; Stammerjohn et al., 2012; Meredith et al., 2013), impacting phytoplankton concentrations (Montes-Hugo et al., 2009) and higher trophic level species such as krill, fish, and Adèlie Penguins (Ducklow et al., 2007, 2012; Schofield et al., 2010). Climate and oceanography trends are also mirrored in the inorganic carbon dynamics, which could feed back to global carbon cycling and/or enhance the projected fast progression of Southern Ocean acidification (McNeil and Matear, 2008; Steinacher et al., 2009; Bopp et al., 2013), thereby imposing additional environmental stressors on the ecosystem.

In the WAP, carbon biogeochemistry is controlled by an interplay of physical and biological mechanisms, which include photosynthesis, respiration, freshwater input, gas exchange, sea-ice cover, winds, and horizontal advection (Carrillo and Karl, 1999; Carrillo et al., 2004; Wang et al., 2009; Montes-Hugo et al., 2010). From austral spring through summer, sea-ice retreats from north to south and from offshore to inshore (Smith and Stammerjohn, 2001). If not counteracted by strong winds, freshwater from melting sea-ice, glaciers and snow (Meredith et al., 2013) stabilizes the water column in close proximity to the inshore and southward moving sea-ice edge. Stratification and iron availability provide favorable conditions for phytoplankton blooms (Garibotti et al., 2003, 2005; Vernet et al., 2008), resulting in a strong drawdown of dissolved inorganic carbon (DIC) and flux of CO_2 from the atmosphere into the ocean (Carrillo et al., 2004; Montes-Hugo et al., 2009; Wang et al., 2009). Subsequent iron depletion results in a decreasing trend of chlorophyll *a* (Chl *a*) from onshore to offshore, with interannual differences in the gradient strength, depending on the onset of the sea-ice retreat, but

BGD
12, 6929–6969, 2015

possibly also the timing of sampling (Garibotti, 2005; Garibotti et al., 2005). In the dark winter months, respiration processes and entrainment of deep CO_2-rich water onto the shelf and into the upper parts of the water column increase the DIC concentration in surface waters to supersaturated levels of CO_2 with respect to the atmosphere (Carrillo et al., 2004; Wang et al., 2009; Tortell et al., 2014).

The inorganic carbon dynamics are further complicated by large-scale atmospheric patterns. The El Niño Southern Oscillation (ENSO) and Southern Annular Mode (SAM) drive the WAP climate and oceanography on a interannual to multidecadal timescale (Yuan and Martinson, 2001; Stammerjohn et al., 2008a). During La Niña years, storms become longer and more intense in the WAP region as a result of a strong low-pressure system driven by the poleward displacement of the polar jet (Yuan, 2004). Positive SAM phases are associated with positive temperature anomalies over the Antarctic Peninsula and decreased sea-ice extent (Kwok, 2002; Stammerjohn et al., 2008). Furthermore, the SAM brings the Southern Hemisphere westerly winds closer to Antarctica, which amplifies the typical features of La Niña. During these periods, nutrient and CO_2-rich Circumpolar Deep Water intrudes more frequently on to the shelf (Martinson et al., 2008). On the other hand, weaker and fewer storms and spatial and temporal extension of sea-ice coverage are observed in negative phases of SAM, with associated stronger stratification of the water column and enhanced biological productivity (Saba et al., 2014). These features are further intensified when a negative SAM coincides with El Niño (Stammerjohn et al., 2008b).

The WAP oceanography and ecosystem has been intensely observed as part of the PAL-LTER (Palmer Long Term Ecological Research) program (http://pal.lternet.edu/) over the past two decades (Ducklow et al., 2007, 2012). Since 1993, this multifaceted data set also contains seawater inorganic carbon measurements taken each January along transects shown in Fig. 1. We complement the summertime inorganic carbon measurements from PAL-LTER with surface underway pCO_2 measurements that cover all four seasons (Takahashi et al., 2013). Here, we describe the spatial, seasonal and interannual variability of the inorganic carbon system over the past two decades with

BGD
12, 6929–6969, 2015

the intention to improve our understanding of the main physical and biological controls. Furthermore, such a uniquely long data set allows us to gain first insights into the impacts of ocean acidification on the region.

2 Data and methods

2.1 In situ data and calculation of carbonate system parameters

We used discrete measurements of seawater DIC, total alkalinity (TA) and nutrients collected during ship-based cruises as part of the PAL-LTER program (protocols at http://pal.lternet.edu/data/), along with temperature and salinity from CTD casts. The data were gathered along the PAL-LTER sampling grid (Fig. 1), which runs 500 km along the coast and 250 km across the shelf. The along shelf transects were spaced every 100 km, with 20 km between the stations of each transect. The data were collected on an annual cruise each January–February from 1993 through 2012. Sample collection and analysis were performed by David Karl and Chris Carrillo for data prior to 2003, by Taro Takahashi in 2003–2004, and by Hugh Ducklow and Matthew Erickson for data in 2005 onward. No TA data were collected during 2003–2004.

Following the WOCE-JGOFS protocols, discrete samples of DIC and TA (300 mL) from Niskin bottle casts were preserved with 200 µL saturated $HgCl_2$ solution and sealed (Dickson and Goyet, 1994). DIC was analyzed by coulometric determination of extracted CO_2 (Johnson et al., 1987). TA was measured with the potentiometric titration method. Certified Reference Materials (provided by A. G. Dickson, Scripps Institution of Oceanography) were used to assure internal consistency of data with a precision of $\pm 2\,\mu mol\,kg^{-1}$ for DIC, $\pm 5\,ueq\,kg^{-1}$ for TA and nutrients of ±1 %. All data are publicly available at http://pal.lternet.edu/.

Calculated pH and saturation state for aragonite (Ω_{arag}) were determined from DIC, TA, temperature, salinity, phosphate, silicate and pressure using the CO2SYS MATLAB-version (van Heuven et al., 2011). To determine the carbonate parameters

BGD
12, 6929–6969, 2015

we applied the dissociation constants for carbonic acid by Dickson and Millero (1987) (refit from Mehrbach et al., 1973). The CO_2 solubility equations of Weiss (1974), and dissociation constants for boric acid by Dickson (1990) were also used to determine pH and Ω_{arag}. pH is reported on the total H^+ ion concentration scale.

The Lamont–Doherty Earth Observatory (LDEO) measured underway-surface pCO_2 with a precision of ±0.5 %, together with salinity and temperature in various seasons between 1999 and 2013, using a shower-type water-gas equilibrator and infrared CO_2 gas analyzer (see http://www.ldeo.columbia.edu/res/pi/CO2/ for the operational and engineering details, Takahashi et al., 2013). A range of five standard gas mixtures spanning between 100 and 700 ppm mole fraction CO_2 certified by the Earth System Research Laboratory of the National Oceanic and Atmospheric Administration (NOAA) was used to calibrate the system every four hours.

2.2 Comparison with deep-water WOCE/CLIVAR inorganic carbon system data

We checked the consistency of the PAL-LTER DIC and TA data by comparing PAL-LTER deep-water (> 2000 m), offshore TA and DIC measurements to deep-water data collected during the World Ocean Circulation Experiment (WOCE) and Climate and Ocean – Variability, Predictability, and Change (CLIVAR) cruises along parts of sections A21 and S4P that were overlapping with the PAL-LTER grid (data available at http://www.nodc.noaa.gov/woce/wdiu/). DIC was measured on all cruises. When necessary, TA was calculated from DIC and either fCO_2 or pCO_2 following the same calculations as described in Sect. 2.1. Figure 2a shows the stations along the WAP where deep-water samples were taken during PAL-LTER and WOCE cruises. PAL-LTER DIC and TA measurements were well within the range of sampled/calculated DIC and TA from the WOCE and CLIVAR cruises (Fig. 2b and c). After removing five outliers, mean deep-water DIC ($DIC^{mean} = 2260.6 \pm 3.8\,\mu mol\,kg^{-1}$) and TA ($TA^{mean} = 2365.4 \pm 7.0\,ueq\,kg^{-1}$) from PAL-LTER cruises corresponded well with the data measured/calculated from WOCE cruises ($DIC^{mean} = 2261.8 \pm 3.0\,\mu mol\,kg^{-1}$; $TA^{mean} = 2365.9 \pm 9.3\,ueq\,kg^{-1}$).

BGD
12, 6929–6969, 2015

2.3 Comparison with underway-surface pCO_2 data

We also undertook a quality check of the PAL-LTER discrete surface DIC and TA data (depth < 5 m) by comparing PAL-LTER pCO_2, which was calculated using observed DIC and TA values, to LDEO pCO_2. LDEO pCO_2 samples that were collected during the PAL-LTER cruises were spatially matched with the PAL-LTER derived pCO_2 values by choosing the nearest latitude and longitude pair within a 1 km distance. PAL-LTER pCO_2 outliers that underestimate/overestimate pCO_2 relative to the underway observations by more than 150 µatm were removed. These outliers included an underestimation of pCO_2 by 188 µatm (DIC underestimation), 194 µatm (DIC underestimation), 174 µatm (TA overestimation) in 2005, 2007 and 2009 respectively, and pCO_2 overestimation relative to the underway observations by as much as 308 µatm in 2005 (DIC overestimation). These outliers were excluded from further analysis. Analysis of the corrected data set with a Linear Regression Type II model suggests a correlation of $r = 0.82$ (Fig. A1a, Table 1). The ranges of pCO_2 values measured in the summers between years 2008 and 2010, and in year 2012 are rather small, which may also introduce a large error on the intercept parameter. The datasets collected in years 2005, 2006, 2007 and 2011 represent a larger range of pCO_2 values, resulting in a slightly better correlation of ($r = 0.89$), with an intercept and slope of -33.4 ± 11.8 and 1.13 ± 0.04 respectively (Fig. A1b, Table 1). Some of the observed discrepancies may also be attributed to errors in matching the time of bottle samples with that of underway pCO_2 measurements. Seawater inorganic carbon chemistry is highly variable along the WAP due to the influence of productivity, respiration, freshwater and upwelling of CO_2-rich subsurface water (Carrillo et al., 2004). Small matching errors may therefore introduce small DIC and TA errors, which would translate into larger fractional errors in pCO_2 due to the large Revelle Factor ($\partial \ln pCO_2 / \partial \ln DIC$) common in the region (Sarmiento and Gruber, 2006).

BGD
12, 6929–6969, 2015

2.4 Salinity based formulation of alkalinity

To take advantage of the LDEO pCO_2, salinity and temperature data set that spans all four seasons from 1999 through 2013, we developed a regional algorithm for TA and calculated pH and Ω_{arag} for fall, winter, spring, and summer from the predicted TA and measured LDEO pCO_2. Since the WAP surface data showed a poor correlation between temperature and TA (Fig. A2, $r = 0.50$), we developed a salinity-based TA algorithm (correlation with S: $r = 0.88$). According to the Akaike information criterion (Burnham and Anderson, 2002), a first order linear model represents the most accurate model to predict TA along the WAP. We then randomly divided the LTER surface measurements (depth < 5 m) into 10 data subsets using the 10-fold cross validation method (Stone, 1974; Breiman, 1996). Using nine of the ten data sets we derived a regression model, predicted the TA with the model, and calculated the model coefficients and root mean square errors (RMSE). We repeated these steps so every data subset was left out once. The coefficients for the final model were calculated from the mean of the ten regression coefficients. We found the best fit in the following equation:

$$TA^{pred}(\text{ueq kg}^{-1}) = 57.01(\pm 0.88) \times S + 373.86(\pm 35.26),$$

which resulted in a linear correlation coefficient of $r = 0.88$ and a RMSE of 15.2 ueq kg^{-1} (Fig. A2). In combination with the pCO_2 measurement precision of 3 uatm, the RMSE of TA prediction resulted in a mean error in predicted Ω_{arag} of 0.02 units (Glover et al., 2011).

3 Results

Here, we examine the observed spatial summer time patterns of DIC, TA, pH and Ω_{arag} along the WAP and explore the underlying biological and physical drivers. We then discuss regional carbon–nutrient drawdown ratios and present our seasonal Ω_{arag} predictions that give initial insights into the chemical environment in the more poorly

BGD
12, 6929–6969, 2015

sampled spring, fall and winter months. Finally, using the LTER and LDEO data sets, we investigate temporal trends over the past two decades.

3.1 Spatial summertime patterns of the inorganic carbon system

The carbon system in the PAL-LTER region exhibited high spatial and interannual variability. To gain a spatial overview of the general summertime surface features (upper 5 m), we linearly interpolated the observations in space and averaged across years with available DIC and TA (or nutrient) measurements. Averages are only shown for regions where samples were taken in more than 5 years (Fig. 3). The resulting pCO_2, pH, Ω_{arag}, TA, salinity, DIC, and nutrient fields exhibited clear onshore–offshore gradients. With the exception of DIC, all parameters also followed a north–south gradient. Mean summertime surface pCO_2 was lowest (< 200 uatm) in the southern coastal region and was about 60 to 70 uatm lower than in the northern near-shore regions (Fig. 3a). The highest mean summertime pCO_2 values were found in the northern slope region (300–325 uatm). The opposite pattern was reflected in Ω_{arag} and pH, with highest values ($\Omega_{arag}^{max} = 2.6$ and $pH^{max} = 8.3$) close to the coast and south of 66.5° S (Fig. 3b and c), decreasing along the coast towards the north to pH ~ 8.2 and $\Omega_{arag} \sim 1.9$, and reaching the lowest levels in northern offshore waters ($pH^{min} = 8.1$; $\Omega_{arag}^{min} = 1.7$). TA also exhibited north–south and onshore–offshore gradients, with values as low as 2185 ueq kg^{-1} in the northern near-shore regions and as high as > 2300 ueq kg^{-1} offshore. The low TA values along the northern part of the coast coincided with the lowest salinity values of 31.8, suggesting dilution of TA due to freshwater input (Fig. 3d and e). Higher TA values offshore were also reflected in increased DIC and salinity concentrations, with temperatures between 1.3–1.5 °C. DIC also exhibited an onshore–offshore gradient with values about 80 to 100 µmol kg^{-1} lower in the near shore region compared to offshore, but there was no significant north–south gradient despite the presence of freshwater in the north (Fig. 3f). Salinity normalized DIC (sDIC, normalized with UCDW salinity = 34.7) was lowest in the southern region, thereby indicating that biological

BGD
12, 6929–6969, 2015

processes likely counteracted the expected north–south DIC gradient due to the pronounced freshwater influence on DIC in the north (Fig. 3g).

The above-presented temporal average of surface Ω_{arag} masks out the large interannual variability and some low levels of surface Ω_{arag} that were close to undersaturation (Fig. 4, min $\Omega_{arag} = 0.97$). Aragonite undersaturation was detected at the surface in 1996 and on the shelf between 100 and 200 m depth in 2005 and 2007. At depths > 70 m, which is below the mixed layer depth, Ω_{arag} was < 1.5 in all years.

3.2 Physical and biological drivers of the inorganic carbon system

In this section we examine the physical and biological mechanisms that control the observed variability in DIC and TA. DIC can be decreased (increased) through dilution with freshwater (evaporation), organic matter production (remineralization), CO_2 outgassing to the atmosphere (CO_2 uptake) and/or precipitation of $CaCO_3$ (dissolution). While positive net community production decreases DIC, the biological effect of organic matter production on TA depends on the source of the nitrogen, where nitrate consumption increases TA and ammonium consumption decreases TA (Goldman and Brewer, 1980). Nitrate is abundant in WAP surface waters, and assuming nitrate as the nitrogen source and a Redfield stoichiometry of 6.6 mol C $(\text{mol N})^{-1}$ then TA should increase by 1/6.6 = +0.15 ueq TA per umol DIC consumed. Precipitation of biological $CaCO_3$ material reduces both DIC and TA with the effect on TA twice as large as that on DIC (2 ueq umol^{-1}). TA is not affected by gas exchange but does vary as a result of dilution and evaporation.

Indications of surface reductions in TA and DIC due to freshwater input are evident along the WAP, and therefore freshwater processes (sea-ice and glacial melt, precipitation) (Meredith et al., 2013) appear to be important factors influencing the summertime carbon dynamics along the WAP. Figure 5 shows TA (circles) and DIC (diamonds) as a function of salinity. The black lines represent the dilution lines for TA and DIC, which were calculated following Yamamoto-Kawai et al. (2009). UCDW end members are based on average TA and DIC concentrations in the water mass identified as UCDW

BGD
12, 6929–6969, 2015

(black frames) (Martinson et al., 2008). Upper-ocean TA follows its dilution line closely, with stronger positive deviations of about 35 ueq kg^{-1} on average. In contrast, DIC values fall considerably below the dilution line. A DIC drawdown of about 60 umol kg^{-1} is visible in the winter water (grey diamonds), which increased to more than 200 umol kg^{-1} in the mixed layer, leading to Ω_{arag} as low as 1.5 and as high as 3.9.

The DIC drawdown relative to the salinity mixing-dilution line is most likely due to biological production of organic matter. Figure 6 shows sDIC as a function of salinity-normalized TA (sTA) for waters shallower than UCDW (orange dots). The regression line (solid black line, sTA = $-0.11 \times$ sDIC + 2601, RMSE = 18.6) $\pm 2\sigma$ (dashed lines) for estimated measurement precision ($\sigma = \pm 5$ ueq kg^{-1}) is similar to the nitrate-based photosynthesis line (blue line), indicating that the large decrease in DIC with the concomitant smaller increase in TA was mainly due to net biological production of organic matter. The photosynthesis line is based on winter water (WW) DIC and TA end-members (blue dots) and a slope of $-1/6.2$. According to the Redfield ratios (C/N/P = 106 : 16 : 1, Redfield, 1958), photosynthetic utilization of 1 mole of NO_3 increases TA by 1 eq kg^{-1} and decreases DIC by 106/16 (6.6). However, since the TA titration was performed to a pH of about 3, the TA values include residual PO_4^{-3}, which leads to this slightly shallower slope of 6.2.

The intense, biologically driven DIC drawdown and resulting pCO_2 undersaturation in the mixed layer may have led to some CO_2 uptake from the atmosphere that tends to reduce the apparent DIC deficit; thus the estimated biological drawdown from observed DIC values in Fig. 6 may be underestimated and needs to be corrected for air–sea CO_2 gas exchange from the period of biological drawdown to the sampling time. To account for DIC concentration changes due to gas exchange with the atmosphere, we assumed a constant atmospheric concentration of 390 uatm between 1993 and 2012, and a gas transfer rate (k) of 5 umol CO_2 m^{-2} $uatm^{-1}$ $month^{-1}$, which is the mean rate over the global oceans based on ^{14}C (Sweeney et al., 2007). The change in DIC (umol kg^{-1} $month^{-1}$) due to gas transfer into the mixed layer (ML) of d meters depth is:

$$\Delta DIC = k \cdot \Delta t \cdot \Delta pCO_2 / d.$$

BGD
12, 6929–6969, 2015

ΔpCO_2 ($pCO_2^{atm} - pCO_2^{ML}$) was between −143 and 312 uatm, as pCO_2^{ML} ranged from 533 to 78 uatm, indicating that there was potential for both oceanic CO_2 uptake and outgassing. Assuming that $d = 50$ m (Ducklow et al., 2013), we estimate that the monthly ΔDIC due to air-to-sea CO_2 gas exchange was in the range of −14 to 31 umol kg^{-1} month^{-1}. Since the first large phytoplankton blooms generally occur after the sea-ice retreats in November ($\Delta t \sim 3$ months), we assume that by the time of sampling at the end of January, ΔDIC would fall in the range −43 to 94 umol kg^{-1}. The DIC corrected for gas exchange is illustrated as grey dots in Fig. 6. While applying the gas exchange correction flattens the regression line (grey line) somewhat, the photosynthesis line (blue) still remains within the estimated error bounds of the gas exchange corrected regression line (grey dotted lines), further emphasizing that photosynthesis is the key biological driver of the summertime carbonate system west of the Antarctic Peninsula.

3.3 Nutrient vs. carbon drawdown

Ocean carbon, nitrogen and phosphorus cycles are governed by organic matter production and subsequent remineralization and are strongly correlated on a global average with the proportions C/N/P = 106 : 16 : 1 (Redfield, 1958). Our findings suggest that the carbon-nutrient cycles along the WAP depart from the standard Redfield values (Fig. 7). In a few samples, the standing stock of PO_4^{3-} became depleted before NO_3^-, and overall the regression indicates a low N : P ratio of 9.8 ± 0.4 in the mixed layer (Fig. 7a, black) and N : P = 11.7 ± 0.3 for all data (dark grey) relative to the standard Redfield value of 16 mol N(mol P)$^{-1}$. The mole/mole C : P ratio was also considerably smaller than the Redfield ratio (Fig. 7b). C : P yielded 43.1 ± 2.3 in the mixed layer and 55.0 ± 1.7 for all data. However, after applying the gas exchange correction on DIC (see Sect. 3.2), the C : P ratio shifted closer to the Redfield Ratio and resulted in a value of 80.5 ± 2.5 (light grey dots and lines). Correcting the DIC for gas exchange shifted the

BGD
12, 6929–6969, 2015

molar ratio from 4.5 ± 0.2 (mixed layer depth) and 4.7 ± 0.1 (all data) to 6.7 ± 0.2 and resulted in a Redfield-like C : N ratio.

3.4 Seasonal variability

In this section we use the LDEO pCO_2, salinity and temperature data set and a salinity-based TA algorithm to predict Ω_{arag} during all seasons between 1999 and 2013 (see Sect. 2.3 for method details). Note that the predicted Ω_{arag} estimates implicitly require that the approximately linear summertime TA-salinity relationship holds for the other seasons, a reasonable assumption if dilution and mixing substantially affect TA patterns. This approach allows for insights into the carbon dynamics during winter, spring, and fall, when direct measurements of DIC and TA are either scarce or not available.

Summertime LDEO underway pCO_2 values were, on average, lower than during the rest of the year (Fig. 8a). The majority of summertime surface LDEO pCO_2 measurements were distributed between 60 and 390 uatm. While less than 1 % of these summertime values reached levels higher than the atmospheric CO_2 concentration, 50 % of the water samples taken in winter were supersaturated with regard to atmospheric CO_2 (> 390 uatm). Spring and fall pCO_2 values were also generally higher than summertime measurements and ranged from 210 to 480 uatm and 180 to 450 uatm.

Our salinity-based algorithm predicted TA with a range of 2200 to 2300 ueq kg^{-1} for fall, winter and spring, with the most frequent occurrence of highest TA in winter and spring (> 40 %, Fig. 8b). Summertime TA was predicted to span a wider range, with a few predictions as low as 1939 ueq kg^{-1}. The majority of the predicted summertime TA values ranged between 2160 and 2300 ueq kg^{-1}, which corresponds with the range that was measured as part of PAL-LTER.

Prediction of seasonal Ω_{arag} revealed that surface waters of the WAP were mostly supersaturated with regard to aragonite throughout the years (Fig. 8c). The most frequent occurrence of low Ω_{arag} was in winter. More than 50 % of the predicted values resulted in $\Omega_{arag} < 1.5$, of which 35 % were $\Omega_{arag} < 1.3$, with the lowest predicted surface Ω_{arag} reaching 0.7. About 20 % of Ω_{arag} predictions were < 1.3 in spring, whereas

BGD
12, 6929–6969, 2015

only 1 % or less of the predictions were < 1.3 in summer and fall. Similar to the LTER observations, predicted summertime Ω_{arag} displayed a large range, spanning from 1.1 to 3.9, with the majority of predictions between 1.3 and 2.

3.5 Temporal trends

Trend analysis of the PAL-LTER data showed no statistically significant annual trends (at the 95 % confidence level) in the measured carbon parameters, temperature or salinity in surface waters between 1993 and 2012 (Table 2).

As a comparison, we conducted the same trend analysis for the LDEO surface underway pCO_2 data set. We divided the LDEO data into a northern and central sub-region, of which the latter corresponds with the area of the LTER-WAP grid. Summertime LDEO observations of the central sub-region also do not show a significant trend in surface pCO_2 (Table 3). However, a significant positive trend was found in fall and spring ($p < 0.05$), when pCO_2 increased by 2.3 (± 0.7) uatm yr^{-1} between 1999 and 2013 in both seasons. The LDEO dataset also suggests that temperature and salinity significantly increased in fall and summer, respectively. In the northern sub-region, which lies outside and north of the LTER-sampling grid, LDEO pCO_2 increased significantly by 1.4 (± 0.5) uatm yr^{-1} in fall. The wintertime surface pCO_2 showed a higher pCO_2 trend (1.7 ± 0.8) uatm yr^{-1}, but this trend was slightly outside the confidence interval and therefore statistically not significant.

4 Discussion

The 20 year-long PAL-LTER seawater inorganic carbon time-series showed a distinct upper-ocean spatial pattern of onshore–offshore and north–south gradients and suggests that the summertime carbon dynamics are primarily controlled by biological productivity and freshwater input in near-shore areas.

BGD
12, 6929–6969, 2015

Surface Ω_{arag} was distributed across a wide range (< 1 to values > 3) in freshwater-influenced areas with salinities $S < 32$ (Fig. 5). To better understand how such a wide range of Ω_{arag} at relatively low salinities was possible, we quantified the effect of freshwater and biological production. Mixing of seawater with sea-ice or glacial meltwater leads to a "dilution" of CO_3^{2-} ions and a decrease in Ω_{arag} because TA and DIC in glacial and sea-ice meltwater are much lower than in seawater (Anderson et al., 2000; Yamamoto-Kawai et al., 2009). Calculations of salinity normalized Ω_{arag} using sDIC and sTA showed that freshwater decreased Ω_{arag} by up to 0.2 units along the coast. Despite the negative effect of freshwater on Ω_{arag}, the water in the south was nevertheless highly supersaturated with $CaCO_3$. The salinity normalized DIC in the near-shore southern region of the PAL-LTER sampling grid was up to 177 µmol kg^{-1} lower than elsewhere, suggesting that near-shore phytoplankton blooms balanced out the negative effect of freshwater on Ω_{arag} and even increased Ω_{arag} by up to 2 units. In 2005, when the above-described pattern was particularly obvious, high Chl *a* (up to 20 ug L^{-1}) in the southern coastal area of the sampling grid provides further evidence that high primary productivity led to the observed high Ω_{arag} despite the presence of freshwater. Similar results were found after the calving event of the Mertz glacier tongue in eastern Antarctica, where enhanced primary productivity increased the Ω_{arag} and thereby counteracted the effect of dilution by meltwater input (Shadwick et al., 2013).

Our findings of onshore–offshore and latitudinal gradients of carbon parameters are supported by previous results that suggest similar patterns for several physical and biogeochemical parameters. Summertime surface temperature, salinity and $NO_3^- + NO_2^-$ are generally lower close to the coast, while Chl *a*, primary production, $Si(OH)_2$ and water column stability decrease from the coast toward the open ocean (Smith, 2001; Garibotti et al., 2003; Vernet et al., 2008). The freshwater along the coast may originate, to a large part, from melting of glacial ice and snow (Meredith et al., 2013). Such glacial and snow-melt plumes have been correlated with increased primary production due to a stabilization of the mixed layer, which creates favorable conditions for phytoplankton blooms (Dierssen et al., 2002). This in turn is thought to be the dominant

BGD
12, 6929–6969, 2015

control of the onshore-offshore gradient of phytoplankton variability and associated biologically-impacted parameters. The north–south gradients possibly reflect the timing of phytoplankton blooms in the north and south. As such, blooms in the north occur sooner than blooms in the south (Smith et al., 2008) – thus on average the PAL-LTER January cruise takes place after the bloom in the north, and during the blooms in the south. This may also be the reason for the nutrient depletion along the coast, despite low biological productivity at the time of sampling in the north (Fig. 3h and i). However, it is important to note that as a result of changes in ice cover, cloud formation and wind over the past 30 years, biological productivity has increased in the southern part of the WAP and significantly decreased north of 63° S (Montes-Hugo et al., 2009). The observed DIC drawdown in the winter water (Figs. 5 and A3) is also supported by previous observations of Chl *a* maxima in the euphotic part of the winter water, likely due to increased iron concentrations there (Garibotti et al., 2003; Garibotti, 2005).

Low Ω_{arag} values (< 1.35) observed offshore overlapped with surface waters supersaturated with regard to atmospheric CO_2, salinities > 33.5, and temperatures between 1.3–1.5 °C. These physical properties are associated with modified UCDW, a mixture between UCDW and Antarctic Surface Water (Smith et al., 1999) and indicate that upwelling of DIC and TA rich water into the mixed layer may lead to lower Ω_{arag} conditions offshore (Carrillo et al., 2004).

The Palmer LTER data indicate N : P uptake ratios lower than the Redfield ratio of 16 : 1, and uptake ratios similar to our findings (14 : 1) are common for the polar region of the Southern Ocean (Weber and Deutsch, 2010; Martiny et al., 2013). Our observed low ratio may be the result of a high abundance of diatoms with low N/P ratios in this cold and nutrient-rich environment (Arrigo, 1999; Arrigo et al., 2002; Green and Sambrotto, 2006; Martiny et al., 2013). Rubin et al., (1998) observed a similar N/P ratio of 13.0 ± 1.2 in the mixed layer south of the Polar Front, and an even lower N/P ratio of 11.3±0.3 was observed in the iron-spiked mixed layer during the iron fertilization experiment in the Subantarctic South Pacific (Hales and Takahashi, 2012). Consistent with the low N/P ratio, the observed C : P ratio (80.5 ± 2.5, corrected for gas exchange) was

BGD
12, 6929–6969, 2015

also smaller than the classic Redfield ratio. This indicates that the regional phosphate cycle shows non-Redfield behavior, which is in agreement with the observed C : P ratio of 91.4 ± 7.9 in the mixed layer south of the Polar Front (Rubin et al., 1998). For the same region, Rubin et al. (1998) describe Redfield behavior of C/N nutrient utilization, which corresponds with our gas exchange corrected C/N nutrient utilization ratio of 6.7 ± 0.2. Recently published work suggests that C/N/P ratios exhibit a latitudinal pattern, with a range of 66 : 11 : 1 to 74 : 13 : 1 at higher latitudes in the Southern Ocean (Martiny et al., 2013) and can therefore be significantly lower than what we found in this study.

TA variability was largely driven by dilution through freshwater input and mixing (Fig. 5), which is well characterized by the salinity-derived TA relationship presented in Sect. 2.4. However, biological mechanisms such as photosynthesis, respiration, $CaCO_3$ precipitation and dissolution also played an important role in controlling TA concentrations in the water column and at the surface (Fig. 6). Neglecting these important drivers may be responsible for the large RMSE of our predicted TA (Fig. A2) relative to other studies that either had additional parameters at hand (i.e. O_2 or nutrients) to derive inorganic carbon system parameters in coastal environments (Juranek et al., 2009; Kim et al., 2010; Evans et al., 2013) or that used salinity algorithms to predict TA in open-ocean regions (Takahashi et al., 2014). Furthermore, TA varied by more than 70 ueq kg^{-1} at salinities > 33.7, which led to an unbalanced distribution of residuals (Fig. A2c). Increasing TA at higher salinities and nearly constant DIC concentrations has been observed before in Arctic and Antarctic regions (Dieckmann et al., 2008; Fransson et al., 2011; Rysgaard et al., 2012; Shadwick et al., 2014) and may be due to formation of ikaite crystals ($CaCO_3.6H_2O$) (Suess et al., 1982) that store TA in sea-ice and, upon melting, release the excess TA into the surface water (Rysgaard et al., 2012, 2013). However, reasons for the observed increasing TA at higher salinities along the WAP remain speculative, since direct evidence of ikaite formation/dissolution such as an increase in DIC associated with TA increase is missing (Fig. 6). A combination of other mechanisms, such as upwelling of high salinity – high TA waters concomitant

BGD
12, 6929–6969, 2015

with biological DIC drawdown, could have increased TA : DIC ratios at high salinities. Finally, the WAP region is very dynamic, with large seasonal changes that may affect the carbon system in ways not representable by one algorithm and may therefore require seasonally adjusted algorithms.

Despite of the above-described shortcomings in our salinity-derived TA algorithm, the predicted Ω_{arag} (Figs. 4 and 8) give a useful overview of the seasonal distribution and variability of Ω_{arag}. Error propagation of pCO_2 measurement precision and TA prediction accuracy suggests that the predicted error for Ω_{arag} may be as little as 0.02 (Glover et al., 2011). The seasonal predictions of Ω_{arag} suggest that some wintertime Ω_{arag} were < 1 and more than a third were between 1.1 and 1.3 (Fig. 9). 25 and 10 % of the predictions made for spring and fall also fell into that category. Short-term exposure to low levels of Ω_{arag} may cause severe dissolution of live pteropod shells and has already been observed in the Scotia Sea (Bednaršek et al., 2012). Surface aragonite undersaturation along the WAP may be a result of ocean acidification and may not have been common at preindustrial times (Hauri et al., 2015).

The strongest and most significant increase in surface pCO_2 was observed in the central sub-region in fall and spring (23 µatm decade^{-1}). This increase is slightly higher than what was found for large areas of the global ocean and the mean atmospheric pCO_2 increase of 19 µatm per decade, which causes a pH decrease of about 0.02 per decade (Takahashi et al., 2014). Interestingly, Stammerjohn et al. (2008a, b) found that sea ice extent and wind are also changing most rapidly in spring and fall, which may enhance sea–air gas exchange and therefore facilitate positive pCO_2 trends. Furthermore, it is likely that the strong counter effect of biological productivity successfully masks out the pCO_2 trend in summer, and decreased gas exchange due to sea ice weakens the trend in winter. Predicted surface pH also decreased in the central sub-region in fall (-0.04 decade^{-1}, $p = 0.003$) and spring (-0.01 decade^{-1}, $p = 0.08$), suggesting first signs of ocean acidification within our sampling record. However, the WAP climate and oceanography are regulated by large-scale atmospheric patterns, such as El Niño Southern Oscillation and Southern Annular Model (Stammerjohn et al., 2008a),

BGD
12, 6929–6969, 2015

which may also influence the region's inorganic carbon chemistry and could therefore be responsible for the observed trends. Additional decades of sampling may be needed in order to be able to distinguish with certainty between natural variability and secular trends (Henson et al., 2010). Furthermore, the precision of predicted pH may not be sufficient to detect the subtle differences between natural variability and anthropogenic trends.

5 Conclusions

This study gives new insights into the spatial and temporal variability of the WAP inorganic carbon system and its main physical and biological drivers. In particular, we found that large inorganic carbon drawdown through biological production in summer caused high near-shore Ω_{arag}, despite glacial and sea-ice melt water input. Furthermore, while summertime inorganic carbon chemistry variables do not show any long-term trends yet, surface pCO_2 has significantly increased in spring and fall over the last 15 years, suggesting first signs of ocean acidification in this highly dynamic and variable system.

Continuation and expansion of the inorganic carbon chemistry timeseries across other seasons is necessary to monitor the progression of ocean acidification, be able to distinguish between natural variability and secular trends and to better understand synergistic effects of ocean acidification and climate change. Due to the region's physical complexity of circulation and forcing, and strong dynamic response to climate variability, we recommend development of a highly resolved biogeochemical model to complement our observational work. Implementation of modeling studies will improve our mechanistic understanding of how interannual variability and anthropogenic climate change impact the inorganic carbon chemistry along the WAP, which is imperative to predict the potential impact on the unique WAP ecosystem.

Author contributions. Designed research: H. W. Ducklow and T. Takahashi. Field sampling and analytical measurements: T. Takahashi, H. W. Ducklow and M. Erickson. Data analysis and

BGD
12, 6929–6969, 2015

interpretation: C. Hauri with help from all co-authors. Wrote the paper: C. Hauri with help from S. C. Doney, T. Takahashi, and H. W. Ducklow.

Acknowledgements. We thank past and present members of the Palmer LTER program as well as the captains and crew of the U.S. Antarctic research vessels. We are especially grateful to Richard Iannuzzi and James Conners for their support with data management. We gladly acknowledge support from the National Science Foundation Polar Programs (NSF OPP-90-11927, OPP-96-32763, OPP-02-17282, OPP-08-23101, and PLR-1440435). This is International Pacific Research Center contribution number 1117.

References

Anderson, S. P., Drever, J. I., Frost, C. D., and Holden, P.: Chemical weathering in the foreland of a retreating glacier, Geochim. Cosmochim. Ac., 64, 1173–1189, doi:10.1016/S0016-7037(99)00358-0, 2000.

Arrigo, K. R.: Phytoplankton community structure and the drawdown of nutrients and CO_2 in the Southern Ocean, Science, 283, 365–367, doi:10.1126/science.283.5400.365, 1999.

Arrigo, K. R.: Taxon-specific differences in C/P and N/P drawdown for phytoplankton in the Ross Sea, Antarctica, Geophys. Res. Lett., 29, 1938, doi:10.1029/2002GL015277, 2002.

Arrigo, K. R., van Dijken, G., and Pabi, S.: Impact of a shrinking Arctic ice cover on marine primary production, Geophys. Res. Lett., 35, L19603, doi:10.1029/2008GL035028, 2008.

Bednaršek, N., Tarling, G. A., Bakker, D. C. E., Fielding, S., Jones, E. M., and Venables, H. J.: Extensive dissolution of live pteropods in the Southern Ocean, Nat. Geosci., 5, 881–885, doi:10.1038/ngeo1635, 2012.

Bopp, L., Resplandy, L., Orr, J. C., Doney, S. C., Dunne, J. P., Gehlen, M., Halloran, P., Heinze, C., Ilyina, T., Séférian, R., Tjiputra, J., and Vichi, M.: Multiple stressors of ocean ecosystems in the 21st century: projections with CMIP5 models, Biogeosciences, 10, 6225–6245, doi:10.5194/bg-10-6225-2013, 2013.

Breiman, L.: Stacked regressions, Mach. Learn., 24, 49–64, doi:10.1007/BF00117832, 1996.

Burnham, K. P. and Anderson, D. R.: Model Selection and Multimodel Inference: A Practical Information-Theoretic Approach, Springer Verlag, New York, 488 pp., 2002.

Carrillo, C. J. and Karl, D. M.: Dissolved inorganic carbon pool dynamics in northern Gerlache Strait, Antarctica, J. Geophys. Res., 104, 15873, doi:10.1029/1999JC900110, 1999.

BGD
12, 6929–6969, 2015

Carrillo, C. J., Smith, R. C., and Karl, D. M.: Processes regulating oxygen and carbon dioxide in surface waters west of the Antarctic Peninsula, Mar. Chem., 84, 161–179, doi:10.1016/j.marchem.2003.07.004, 2004.

Dickson, A. G.: Thermodynamics of the dissociation of boric acid in synthetic seawater from 273.15 to 318.15 K, Deep-Sea Res., 37, 755–766, doi:10.1016/0198-0149(90)90004-F, 1990.

Dickson, A. G. and Goyet, C.: Handbook of Methods for the Analysis of the Various Parameters of the Carbon Dioxide System in Sea Water, ORNL/CDIAC-74, 1994.

Dickson, A. G. and Millero, F. J.: A comparison of the equilibrium constants for the dissociation of carbonic acid in seawater media, Deep-Sea Res., 34, 1733–1743: doi:10.1016/0198-0149(87)90021-5, 1987.

Dieckmann, G. S., Nehrke, G., Papadimitriou, S., Göttlicher, J., Steininger, R., Kennedy, H., Wolf-Gladrow, D., and Thomas, D. N.: Calcium carbonate as ikaite crystals in Antarctic sea ice, Geophys. Res. Lett., 35, L08501, doi:10.1029/2008GL033540, 2008.

Dierssen, H. M., Smith, R. C., and Vernet, M.: Glacial meltwater dynamics in coastal waters west of the Antarctic peninsula, Proc. Natl. Acad. Sci. USA, 99, 1790–1795, doi:10.1073/pnas.032206999, 2002.

Ducklow, H., Fraser, W., Meredith, M., Stammerjohn, S., Doney, S., Martinson, D., Sailley, S., Schofield, O., Steinberg, D., Venables, H., and Amsler, Ch.: West Antarctic Peninsula: an ice-dependent coastal marine ecosystem in transition, Oceanography, 26, 190–203, doi:10.5670/oceanog.2013.62, 2013.

Ducklow, H. W., Baker, K., Martinson, D. G., Quetin, L. B., Ross, R. M., Smith, R. C., Stammerjohn, S. E., Vernet, M., and Fraser, W.: Marine pelagic ecosystems: the West Antarctic Peninsula, Philos. Trans. R. Soc. B Biol. Sci., 362, 67–94, doi:10.1098/rstb.2006.1955, 2007.

Ducklow, H. W., Clarke, A., Dickhut, R., Doney, S. C., Geisz, H., Kuan H., Martinson, D. G., Schofield, O. M. E., Stammerjohn, S. E., Steinberg, D. K., and Fraser, W. R.: The marine system of the Western Antarctic Peninsula, in: Antarctic Ecosystems: An Extreme Environment in a Changing World, edited by: Rogers, A. D., Johnston, N. M., Murphy, E. J., and Clarke, A., John Wiley & Sons, Ltd., 2012.

Evans, W., Mathis, J. T., Winsor, P., Statscewich, H., and Whitledge, T. E.: A regression modeling approach for studying carbonate system variability in the northern Gulf of Alaska, J. Geophys. Res. Ocean., 118, 476–489, doi:10.1029/2012JC008246, 2013.

BGD
12, 6929–6969, 2015

Fransson, A., Chierici, M., Yager, P. L., and Smith, W. O.: Antarctic sea ice carbon dioxide system and controls, J. Geophys. Res., 116, C12035, doi:10.1029/2010JC006844, 2011.
Garibotti, I., Vernet, M., Ferrario, M., Smith, R., Ross, R., and Quetin, L.: Phytoplankton spatial distribution patterns along the western Antarctic Peninsula (Southern Ocean), Mar. Ecol.-Prog. Ser., 261, 21–39, doi:10.3354/meps261021, 2003.
Garibotti, I. A.: Interannual variability in the distribution of the phytoplankton standing stock across the seasonal sea-ice zone west of the Antarctic Peninsula, J. Plankton Res., 27, 825–843, doi:10.1093/plankt/fbi056, 2005.
Garibotti, I. A., Vernet, M., and Ferrario, M. E.: Annually recurrent phytoplanktonic assemblages during summer in the seasonal ice zone west of the Antarctic Peninsula (Southern Ocean), Deep-Sea Res., 52, 1823–1841, doi:10.1016/j.dsr.2005.05.003, 2005.
Glover, D., Jenkins, W., and Doney, S.: Modeling Methods for Marine Science, 1st ed., Cambridge University Press, New York, 571 pp., 2011.
Goldman, J. and Brewer, P. G.: Effect of nitrogen source and growth rate on phytoplankton-mediated changes in alkalinity, Limnol. Oceanogr., 25, 352–357, doi:10.4319/lo.1980.25.2.0352, 1980.
Green, S. E. and Sambrotto, R. N.: Plankton community structure and export of C, N, P and Si in the Antarctic Circumpolar Current, Deep-Sea Res., 53, 620–643, doi:10.1016/j.dsr2.2006.01.022, 2006.
Hales, B. and Takahashi, T.: Mesoscale biogeochemical responses to iron fertilization in the upper layers of the Southern Ocean Iron Experiment areas, J. Geophys. Res., 117, C01018, doi:10.1029/2011JC006956, 2012.
Hauri, C., Friedrich, T., and Timmermann, A.: Abrupt onset and prolongation of aragonite undersaturation events in the Southern Ocean, submitted, 2015.
Henson, S. A., Sarmiento, J. L., Dunne, J. P., Bopp, L., Lima, I., Doney, S. C., John, J., and Beaulieu, C.: Detection of anthropogenic climate change in satellite records of ocean chlorophyll and productivity, Biogeosciences, 7, 621–640, doi:10.5194/bg-7-621-2010, 2010.
Johnson, K., Sieburth, J. M., Williams, P. J. leB, and Brändström, L.: Coulometric total carbon dioxide analysis for marine studies: automation and calibration, Mar. Chem., 21, 117–133, doi:10.1016/0304-4203(87)90033-8, 1987.
Juranek, L. W., Feely, R. A., Peterson, W. T., Alin, S. R., Hales, B., Lee, K., Sabine, C. L., and Peterson, J.: A novel method for determination of aragonite saturation state on the continental

BGD
12, 6929–6969, 2015

shelf of central Oregon using multi-parameter relationships with hydrographic data, Geophys. Res. Lett., 36, L24601, doi:10.1029/2009GL040778, 2009.

Kim, T.-W., Lee, K., Feely, R. A., Sabine, C. L., Chen, C.-T. A., Jeong, H. J., and Kim, K. Y.: Prediction of Sea of Japan (East Sea) acidification over the past 40 years using a multiparameter regression model, Global Biogeochem. Cy., 24, GB3005, doi:10.1029/2009GB003637, 2010.

Kwok, R.: Spatial patterns of variability in Antarctic surface temperature: connections to the Southern Hemisphere Annular Mode and the Southern Oscillation, Geophys. Res. Lett., 29, 1705, doi:10.1029/2002GL015415, 2002.

Martinson, D. G., Stammerjohn, S. E., Iannuzzi, R. A., Smith, R. C., and Vernet, M.: Western Antarctic Peninsula physical oceanography and spatio–temporal variability, Deep-Sea Res., 55, 1964–1987, doi:10.1016/j.dsr2.2008.04.038, 2008.

Martiny, A. C., Pham, C. T. A., Primeau, F. W., Vrugt, J. A., Moore, J. K., Levin, S. A., and Lomas, M. W.: Strong latitudinal patterns in the elemental ratios of marine plankton and organic matter, Nat. Geosci., 6, 279–283, doi:10.1038/ngeo1757, 2013.

McNeil, B. I. and Matear, R. J.: Southern Ocean acidification: a tipping point at 450-ppm atmospheric CO_2, Proc. Natl. Acad. Sci. USA, 105, 18860–18864, doi:10.1073/pnas.0806318105, 2008.

Mehrbach, C., Culberson, C. H., Hawley, J. E., and Pytkowicz, R. M.: Measurement of the apparent dissociation constants of carbonic acid in seawater at atmospheric pressure, Limnol. Oceanogr., 18, 897–907, doi:10.4319/lo.1973.18.6.0897, 1973.

Meredith, M. P., Venables, H. J., Clarke, A., Ducklow, H. W., Erickson, M., Leng, M. J., Lenaerts, J. T. M., and van den Broeke, M. R.: The Freshwater System West of the Antarctic Peninsula: spatial and temporal changes, J. Climate, 26, 1669–1684, doi:10.1175/JCLI-D-12-00246.1, 2013.

Montes-Hugo, M., Doney, S. C., Ducklow, H. W., Fraser, W., Martinson, D., Stammerjohn, S. E., and Schofield, O.: Recent changes in phytoplankton communities associated with rapid regional climate change along the western Antarctic Peninsula, Science, 323, 1470–1473, doi:10.1126/science.1164533, 2009.

Montes-Hugo, M., Sweeney, C., Doney, S. C., Ducklow, H., Frouin, R., Martinson, D. G., Stammerjohn, S., and Schofield, O.: Seasonal forcing of summer dissolved inorganic carbon and chlorophyll *a* on the western shelf of the Antarctic Peninsula, J. Geophys. Res., 115, C03024, doi:10.1029/2009JC005267, 2010.

BGD
12, 6929–6969, 2015

Redfield, A.: The biological control of chemical factors in the environment, Am. Sci., 3, 205–221, 1958.
Rubin, S. I., Takahashi, T., Chipman, D. W., and Goddard, J. G.: Primary productivity and nutrient utilization ratios in the Pacific sector of the Southern Ocean based on seasonal changes in seawater chemistry, Deep-Sea Res., 45, 1211–1234, doi:10.1016/S0967-0637(98)00021-1, 1998.
Rysgaard, S., Glud, R. N., Lennert, K., Cooper, M., Halden, N., Leakey, R. J. G., Hawthorne, F. C., and Barber, D.: Ikaite crystals in melting sea ice – implications for pCO_2 and pH levels in Arctic surface waters, The Cryosphere, 6, 901–908, doi:10.5194/tc-6-901-2012, 2012.
Rysgaard, S., Søgaard, D. H., Cooper, M., Pućko, M., Lennert, K., Papakyriakou, T. N., Wang, F., Geilfus, N. X., Glud, R. N., Ehn, J., McGinnis, D. F., Attard, K., Sievers, J., Deming, J. W., and Barber, D.: Ikaite crystal distribution in winter sea ice and implications for CO_2 system dynamics, The Cryosphere, 7, 707–718, doi:10.5194/tc-7-707-2013, 2013.
Saba, G. K., Fraser, W. R., Saba, V. S., Iannuzzi, R. A., Coleman, K. E., Doney, S. C., Ducklow, H. W., Martinson, D. G., Miles, T. N., Patterson-Fraser, D. L., Stammerjohn, S. E., Steinberg, D. K., and Schofield, O. M.: Winter and spring controls on the summer food web of the coastal West Antarctic Peninsula., Nat. Commun., 5, 4318, doi:10.1038/ncomms5318, 2014.
Sarmiento, J. L. and Gruber, N.: Ocean Biogeochemical Dynamics, Princeton University Press, Princeton, NJ, 528 pp., 2006.
Schofield, O., Ducklow, H. W., Martinson, D. G., Meredith, M. P., Moline, M. A., and Fraser, W. R.: How do polar marine ecosystems respond to rapid climate change?, Science, 328, 1520–1523, doi:10.1126/science.1185779, 2010.
Shadwick, E. H., Rintoul, S. R., Tilbrook, B., Williams, G. D., Young, N., Fraser, A. D., Marchant, H., Smith, J., and Tamura, T.: Glacier tongue calving reduced dense water formation and enhanced carbon uptake, Geophys. Res. Lett., 40, 904–909, doi:10.1002/grl.50178, 2013.
Shadwick, E. H., Tilbrook, B., and Williams, G. D.: Carbonate chemistry in the Mertz Polynya (East Antarctica): biological and physical modification of dense water outflows and the export of anthropogenic CO_2, J. Geophys. Res. Ocean., 119, 1–14, doi:10.1002/2013JC009286, 2014.

BGD
12, 6929–6969, 2015

Smith, D. A., Hofmann, E. E., Klinck, J. M., and Lascara, C. M.: Hydrography and circulation of the West Antarctic Peninsula Continental Shelf, Deep-Sea Res., 46, 925–949, doi:10.1016/S0967-0637(98)00103-4, 1999.

Smith, R. C.: Variability of primary production in an Antarctic marine ecosystem as estimated using a multi-scale sampling strategy, Integr. Comp. Biol., 41, 40–56, doi:10.1093/icb/41.1.40, 2001.

Smith, R. C. and Stammerjohn, S. E.: Variations of surface air temperature and sea-ice extent in the western Antarctic Peninsula region, Ann. Glaciol., 33, 493–500, doi:10.3189/172756401781818662, 2001.

Smith, R. C., Martinson, D. G., Stammerjohn, S. E., Iannuzzi, R. A., and Ireson, K.: Bellingshausen and western Antarctic Peninsula region: pigment biomass and sea-ice spatial/temporal distributions and interannual variabilty, Deep-Sea Res., 55, 1949–1963, doi:10.1016/j.dsr2.2008.04.027, 2008.

Stammerjohn, S., Massom, R., Rind, D., and Martinson, D.: Regions of rapid sea ice change: an inter-hemispheric seasonal comparison, Geophys. Res. Lett., 39, L06501, doi:10.1029/2012GL050874, 2012.

Stammerjohn, S. E., Martinson, D. G., Smith, R. C., and Iannuzzi, R. A.: Sea ice in the western Antarctic Peninsula region: spatio-temporal variability from ecological and climate change perspectives, Deep-Sea Res., 55, 2041–2058, doi:10.1016/j.dsr2.2008.04.026, 2008a.

Stammerjohn, S. E., Martinson, D. G., Smith, R. C., Yuan, X., and Rind, D.: Trends in Antarctic annual sea ice retreat and advance and their relation to El Niño–Southern Oscillation and Southern Annular Mode variability, J. Geophys. Res., 113, C03S90, doi:10.1029/2007JC004269, 2008b.

Steinacher, M., Joos, F., Frölicher, T. L., Plattner, G.-K., and Doney, S. C.: Imminent ocean acidification in the Arctic projected with the NCAR global coupled carbon cycle-climate model, Biogeosciences, 6, 515–533, doi:10.5194/bg-6-515-2009, 2009.

Stone, M.: Cross-validatory choice and assessment of statistical predictions, J. Roy. Stat. Soc. B. Met., 36, 111–147, 1974.

Suess, E., Balzer, W., Hesse, K. F., Müller, P. J., Ungerer, C. A., and Wefer, G.: Calcium carbonate hexahydrate from organic-rich sediments of the antarctic shelf: precursors of glendonites, Science, 216, 1128–1131, doi:10.1126/science.216.4550.1128, 1982.

BGD
12, 6929–6969, 2015

Sweeney, C., Gloor, E., Jacobson, A. R., Key, R. M., McKinley, G., Sarmiento, J. L., and Wanninkhof, R.: Constraining global air–sea gas exchange for CO_2 with recent bomb 14C measurements, Global Biogeochem. Cy., 21, GB2015, doi:10.1029/2006GB002784, 2007.

Takahashi, T., Sutherland, S. C., and Kozyr, A.: Global ocean surface water partial pressure of CO_2 database: measurements performed during 1957–2012 (Version 2012), ORNL/CDIAC-160, NDP-088(V2012), Carbon Dioxide Inf. Anal. Center, Oak Ridge Natl. Lab. U.S. Dep. Energy, Oak Ridge, Tennessee, doi:10.3334/CDIAC/OTG.NDP088(V2012), 2013.

Takahashi, T., Sutherland, S. C., Chipman, D. W., Goddard, J. G., Ho, C., Newberger, T., Sweeney, C., and Munro, D. R.: Climatological distributions of pH, pCO_2, total CO_2, alkalinity, and $CaCO_3$ saturation in the global surface ocean, and temporal changes at selected locations, Mar. Chem., 164, 95–125, doi:10.1016/j.marchem.2014.06.004, 2014.

Tortell, P. D., Asher, E. C., Ducklow, H. W., Goldman, J. A. L., Dacey, J. W. H., Grzymski, J. J., Young, J. N., Kranz, S. A., Bernard, K. S., and Morel, F. M. M.: Metabolic balance of coastal Antarctic waters revealed by autonomous pCO_2 and δO_2/Armeasurements, Geophys. Res. Lett., 41, 6803–6810, doi:10.1002/2014GL061266, 2014.

Van Heuven, S., Pierrot, D., Rae, J. W. B., Lewis, E., and Wallace, D. W. R.: MATLAB Program Developed for CO_2 System Calculations, ORNL/CDIAC-105b, Carbon Dioxide Information Analysis Center, Oak Ridge National Laboratory, U.S. Department of Energy, Oak Ridge, Tennessee, doi:10.3334/CDIAC/otg.CO2SYS_MATLAB_v1.1, 2011.

Vernet, M., Martinson, D., Iannuzzi, R., Stammerjohn, S., Kozlowski, W., Sines, K., Smith, R., and Garibotti, I.: Primary production within the sea-ice zone west of the Antarctic Peninsula, I – sea ice, summer mixed layer, and irradiance, Deep-Sea Res., 55, 2068–2085, doi:10.1016/j.dsr2.2008.05.021, 2008.

Wang, X., Yang, G.-P., López, D., Ferreyra, G., Lemarchand, K., and Xie, H.: Late autumn to spring changes in the inorganic and organic carbon dissolved in the water column at Scholaert Channel, West Antarctica, Antarct. Sci., 22, 145, doi:10.1017/S0954102009990666, 2009.

Weber, T. S. and Deutsch, C.: Ocean nutrient ratios governed by plankton biogeography, Nature, 467, 550–554, doi:10.1038/nature09403, 2010.

Weiss, R.: Carbon dioxide in water and seawater: the solubility of a non-ideal gas, Mar. Chem., 2, 203–215, doi:10.1016/0304-4203(74)90015-2, 1974.

BGD
12, 6929–6969, 2015

Yamamoto-Kawai, M., McLaughlin, F. A., Carmack, E. C., Nishino, S., and Shimada, K.: Aragonite undersaturation in the Arctic Ocean: effects of ocean acidification and sea ice melt, Science, 326, 1098–1100, doi:10.1126/science.1174190, 2009.

Yuan, X.: ENSO-related impacts on Antarctic sea ice: a synthesis of phenomenon and mechanisms, Antarct. Sci., 16, 415–425, doi:10.1017/S0954102004002238, 2004.

Yuan, X. and Martinson, D. G.: The Antarctic dipole and its predictability, Geophys. Res. Lett., 28, 3609–3612, doi:10.1029/2001GL012969, 2001.

BGD
12, 6929–6969, 2015

Table 1. Statistics for comparison of Lamont–Doherty Earth Observatory of Columbia University (LDEO) underway pCO_2 (uatm) data (Takahashi et al., 2013) with the pCO_2 (uatm) derived from PAL-LTER discrete surface samples over the Palmer-Long Term Ecological Research (PAL-LTER) sampling grid. The PAL-LTER discrete pCO_2 sample values were computed using the dissolved inorganic carbon (DIC, umol kg^{-1}) and total alkalinity (TA, ueq kg^{-1}). The analysis is based on the data after removing outliers as explained in the text. Years used in the second analysis shown in Fig. A1b are marked with *.

		Mean (SD)	r	Slope	Intercept	n
2005*	LDEO	293 (78)	0.94	1.05 (±0.06)	−44.7 (±18.1)	49
	PAL-LTER	322 (75)				
2006*	LDEO	248 (46)	0.90	0.95 (±0.06)	12.4 (±15.6)	55
	PAL-LTER	248 (48)				
2007*	LDEO	261 (60)	0.87	1.03 (±0.08)	15.9 (±18.3)	60
	PAL-LTER	237 (59)				
2008	LDEO	340 (28)	0.53	0.62 (±0.14)	156 (±42.2)	48
	PAL-LTER	299 (37)				
2009	LDEO	318 (24)	0.56	0.47 (±0.13)	179 (±38.0)	27
	PAL-LTER	292 (37)				
2010	LDEO	327 (35)	0.54	1.60 (±0.56)	−161 (±170)	20
	PAL-LTER	305 (27)				
2011*	LDEO	227 (97)	0.93	0.96 (±0.08)	2.23 (±21.2)	21
	PAL-LTER	233 (101)				
2012	LDEO	354 (36)	0.45	1.45 (±0.63)	50.0 (±175)	21
	PAL-LTER	279 (30)				
All	LDEO	290 (68)	0.82	1.07 (±0.04)	−4.81 (±12.2)	300
	PAL-LTER	275 (65)				
Years with*	LDEO	261 (70)	0.89	0.92 (±0.04)	19.8 (9.39)	184
	PAL-LTER	262 (75)				

BGD
12, 6929–6969, 2015

Table 2. Mean annual trend (1993–2012) of Palmer-Long Term Ecological Research (PAL-LTER) surface (depth < 5 m) carbonate chemistry and hydrography from the Western Antarctic Peninsula. Regression statistics include the mean annual rate (yr^{-1}), standard error (SE), number of measurements (NM), number of years (NY), *r*-square, and *p* value for aragonite saturation state (Ω_{arag}), pH, dissolved inorganic carbon (DIC, $umol\,kg^{-1}$), total alkalinity (TA, $ueq\,kg^{-1}$), temperature (°C), and salinity. Trends with a *p* value < 0.05 are statistically significant at the 95 % confidence level (values bolded). Points that were outliers at 95 % probability level were excluded (o).

Parameter Surface (< 5 m depth)	Rate (yr^{-1}) ± SE	NM(o)	NY	r^2	*p* value
Ω_{arag}	0.001 ± 0.01	892(17)	18	0.04	0.9127
pH	0.002 ± 0.002	892(8)	18	0.03	0.2784
DIC ($umol\,kg^{-1}$)	−0.18 ± 1.03	907(0)	18	0.00	0.8677
TA ($ueq\,kg^{-1}$)	0.58 ± 0.63	907(0)	18	0.05	0.3681
Temperature (°C)	−0.01 ± 0.02	1076(8)	20	0.01	0.4629
Salinity	0.01 ± 0.01	1060(8)	20	0.12	0.1349

BGD
12, 6929–6969, 2015

Table 3. Trend analysis (1999–2013) of Lamont–Doherty Earth Observatory of Columbia University (LDEO) surface continuous underway pCO_2 (uatm), salinity and temperature (°C) measurements from within the Palmer-Long Term Ecological Research (PAL-LTER) sampling grid (central subregion, 63.8 to 67.8° S, 64.4 to 73.0° W) and along the northern part of the WAP (61.8 to 64.5° S, 59.0 to 65.8° W). Subregions are marked in Fig. 1. Regression statistics include mean rate, standard error (SE), number of measurements (NM), number of years (NY), r-square, and p value. Trends with a p value < 0.05 are statistically significant at the 95 % confidence level (bold numbers).

Parameter	Season	Rate ± SE	NM	NY	r^2	p value
Central sub-region						
pCO_2 (uatm yr^{-1})	Summer	1.28 ± 2.87	138 479	12	0.02	0.6659
	Fall	2.32 ± 0.70	90 858	15	0.46	**0.0055**
	Winter	0.01 ± 0.77	54 785	14	0.03	0.9940
	Spring	2.29 ± 0.67	49 503	14	0.21	**0.0059**
Temperature (°C yr^{-1})	Summer	0.00 ± 0.03	138 533	12	0.04	0.9096
	Fall	0.15 ± 0.05	90 826	15	0.31	**0.0070**
	Winter	0.07 ± 0.09	54 805	12	0.13	0.4500
	Spring	0.00 ± 0.08	49 493	14	0.00	0.9705
Salinity (yr^{-1})	Summer	0.05 ± 0.01	113 096	12	0.54	**0.0034**
	Fall	0.02 ± 0.01	110 777	15	0.14	0.0584
	Winter	0.01 ± 0.01	48 407	13	0.07	0.4218
	Spring	0.00 ± 0.01	59 354	14	0.05	0.8217
Northern sub-region						
pCO_2 (uatm yr^{-1})	Summer	1.30 ± 0.85	88 581	13	0.36	0.1574
	Fall	1.38 ± 0.47	143 394	15	0.41	**0.0116**
	Winter	1.70 ± 0.79	64 380	14	0.28	0.0530
	Spring	−0.29 ± 0.66	111 857	14	0.02	0.6656
Temperature (°C yr^{-1})	Summer	0.02 ± 0.05	88 631	13	0.25	0.7415
	Fall	0.11 ± 0.05	143 340	15	0.11	0.0580
	Winter	0.00 ± 0.07	64 220	14	0.03	0.9989
	Spring	0.14 ± 0.07	111 879	14	0.23	0.0803
Salinity (yr^{-1})	Summer	−0.01 ± 0.01	115 753	13	0.01	0.4981
	Fall	0.00 ± 0.01	132 737	15	0.01	0.7305
	Winter	0.02 ± 0.01	61 180	12	0.27	0.0566
	Spring	0.01 ± 0.01	89 244	13	0.01	0.5390

BGD
12, 6929–6969, 2015

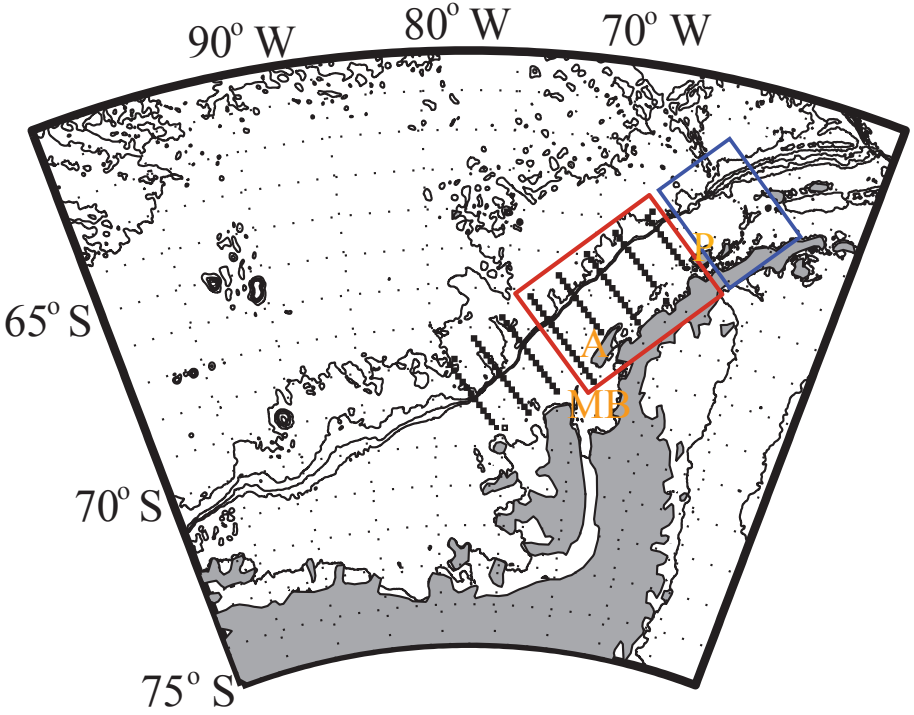

Figure 1. Map of the Western Antarctic Peninsula (WAP) and study area of the Palmer Station Long Term Ecological Research (PAL-LTER) project. The red box shows the main study grid that has been sampled for inorganic carbon chemistry since 1993, and is defined in this study as the central sub-region. The black squares indicate the stations (20 km apart) arranged in onshore to offshore lines spaced 100 km apart along the peninsula. The inorganic carbon measurements from stations south of the central sub region were only added in 2009. Both, the central and northern sub-regions (blue box) contain surface underway pCO_2 observations and were used in the trend analysis (Sect. 3.5). P: Palmer Station on Anvers Island; A: Adelaide Island; and MB: Marguerite Bay.

BGD
12, 6929–6969, 2015

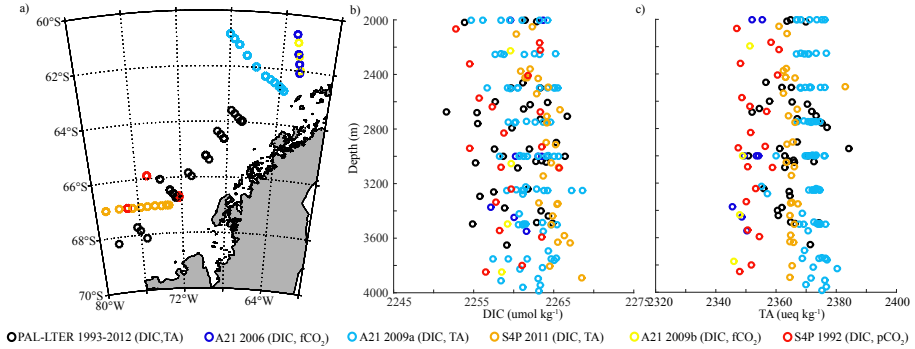

Figure 2. Comparison of deep-water (off shelf) dissolved inorganic carbon (DIC, umol kg^{-1}) and total alkalinity (TA, ueq kg^{-1}) data from Palmer Station Long Term Ecological Research (PAL-LTER) with other available cruise data. **(a)** Station locations, **(b)** DIC and **(c)** TA depth profiles from PAL-LTER cruises (1998–2012), World Ocean Circulation Experiment (WOCE) Sections A21 (2006, 2009) and S4P (1992, 2011). The directly measured parameters are listed in the parentheses and were used to calculate TA if not directly measured.

BGD
12, 6929–6969, 2015

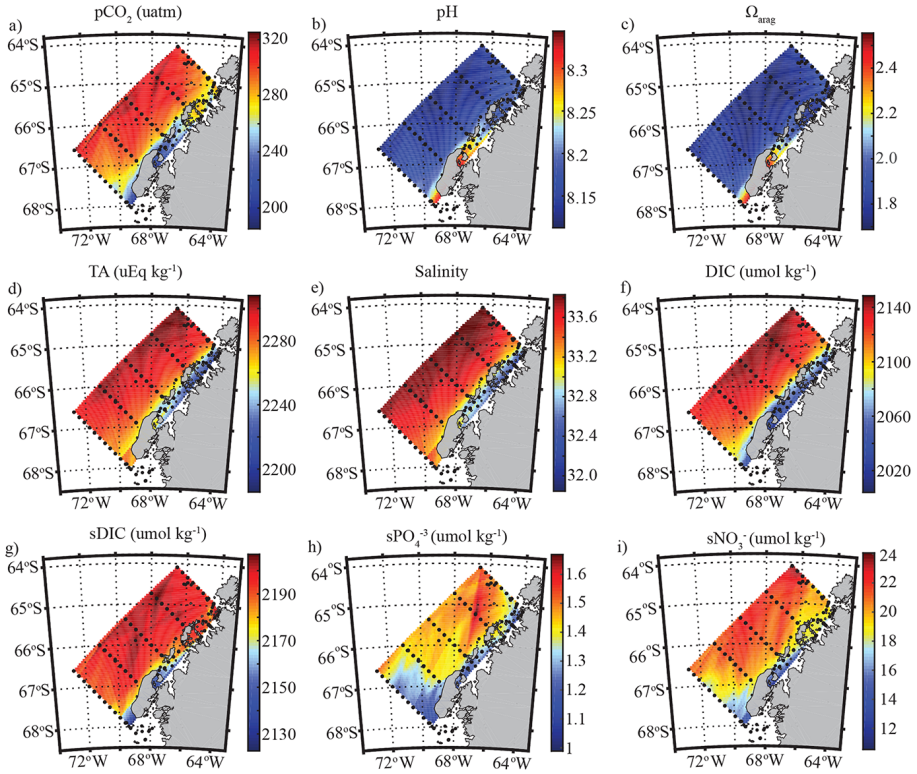

Figure 3. Maps of summertime averages of surface **(a)** pCO_2, **(b)** pH, **(c)** aragonite saturation state (Ω_{arag}), **(d)** total alkalinity (TA, ueq kg^{-1}), **(e)** salinity, **(f)** dissolved inorganic carbon (DIC, umol kg^{-1}), and **(g)** salinity-normalized DIC (sDIC, umol kg^{-1}) across years with available DIC and TA measurements (1993–1999, 2001–2002, and 2005–2012). Salinity-normalized PO_4^{3-} (sPO_4^{3-}, umol kg^{-1}) and salinity normalized NO_3^- (sNO_3^-, umol kg^{-1}) were avaeraged across 1993–1996, 1999, and 2001–2012. Averages are only shown for regions where samples were taken in more than five years. Occupied stations are shown by black dots.

BGD
12, 6929–6969, 2015

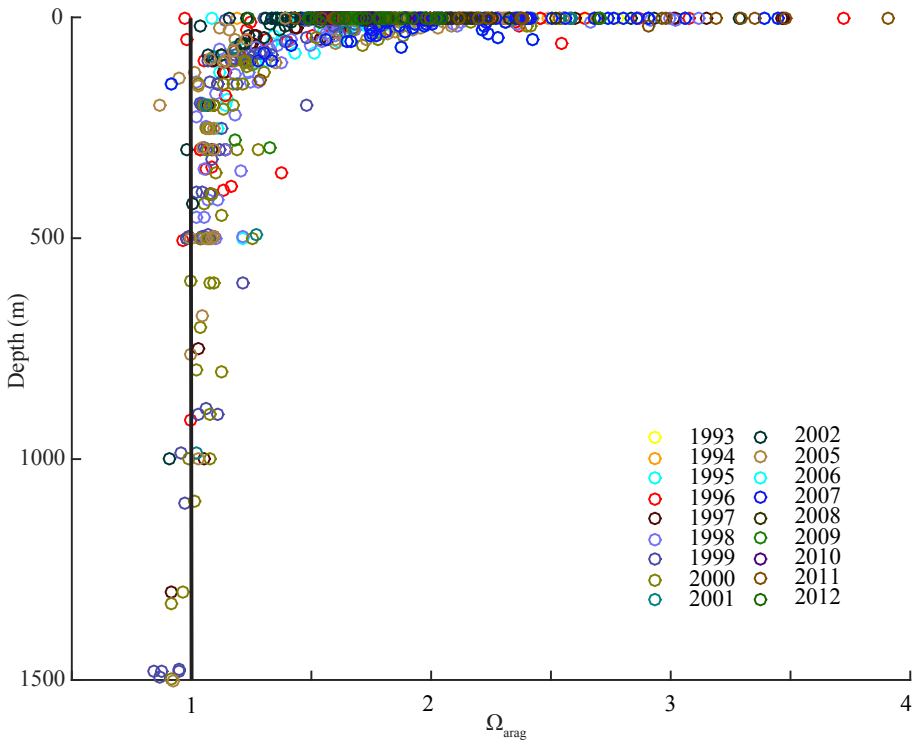

Figure 4. Depth profiles of aragonite saturation state (Ω_{arag}) estimated for the years 1993 through 2012. The aragonite saturation horizon for each year is located where the profile crosses the black line (Ω_{arag} = 1.0).

BGD
12, 6929–6969, 2015

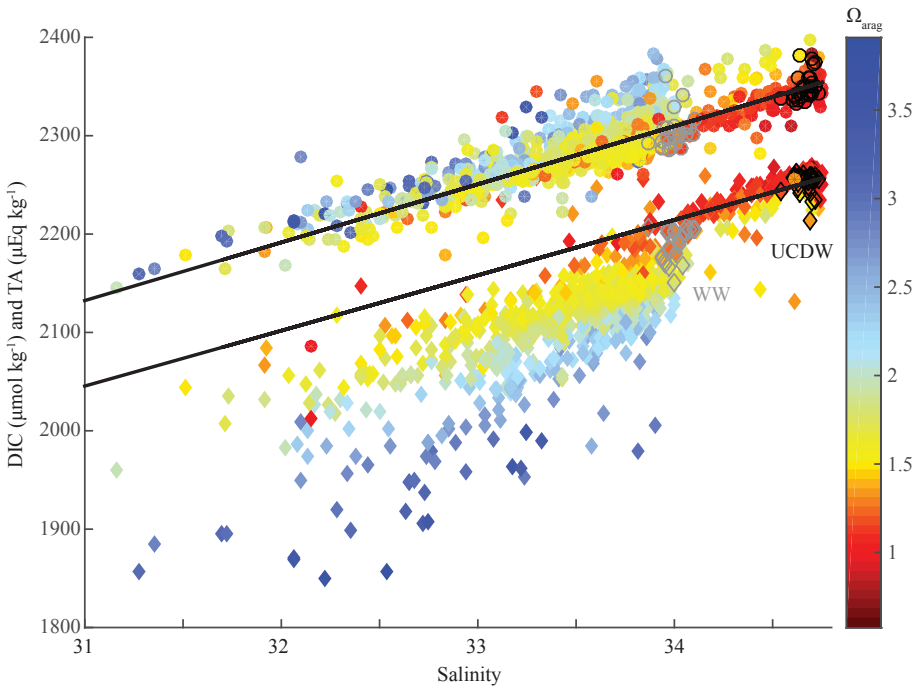

Figure 5. Physical and biological controls of inorganic carbon chemistry. Scatter plots of dissolved inorganic carbon (DIC, umol kg^{-1}) illustrated as diamonds and total alkalinity (TA, ueq kg^{-1}) illustrated as dots as a function of salinity. The data points are color coded by the aragonite saturation state (Ω_{arag}). The solid lines illustrate the dilution lines using $S = 34.7$, TA = 2350 ueq kg^{-1}, and DIC = 2253 umol kg^{-1} as end members for UCDW, and $S = 0$, TA = 300 ueq kg^{-1}, and DIC = 300 umol kg^{-1} as end members for melt water (Yamamoto-Kawai et al., 2009b). WW = Winter water ($T \leq -1.2$; $33.85 \leq S \leq 34.13$), UCDW = Upper Circumpolar Deep Water ($1.7 \leq T \leq 2.13$; $34.54 \leq S \leq 34.75$) following (Martinson et al., 2008).

BGD
12, 6929–6969, 2015

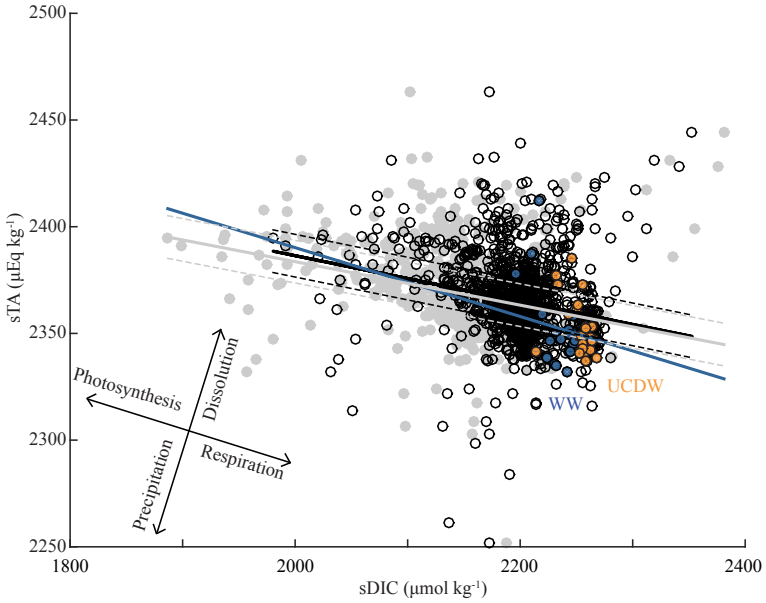

Figure 6. Biological controls of inorganic carbon chemistry. **(a)** Salinity-normalized total alkalinity (sTA, ueq kg^{-1}) as a function of salinity-normalized dissolved inorganic carbon (sDIC, umol kg^{-1}) for waters shallower than the Upper Circumpolar Deep Water (UCDW, black circles). A linear fit between sTA and sDIC is shown by the black solid line. The dotted black lines indicate 2σ for estimated measurement precision of $\sigma = \pm 5$ ueq kg^{-1}. The blue line illustrates the trend if sTA and sDIC of the winter water (WW) were only influenced by photosynthesis (1 : −6.2). Grey dots represent sTA as a function of sDIC corrected for gas exchange in the waters above the WW, and the linear fits with the estimated measurement precision are the grey solid and dashed lines respectively. WW: $T \leq -1.2$; $33.85 \leq S \leq 34.13$, UCSW: $1.7 \leq T \leq 2.13$; $34.54 \leq S \leq 34.75$, following (Martinson et al., 2008).

BGD
12, 6929–6969, 2015

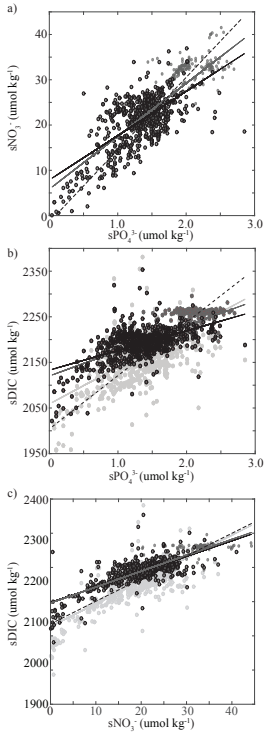

Figure 7. Nutrient consumption. Plot of salinity-normalized nutrients and dissolved inorganic carbon (*s*DIC), **(a)** sPO_4^{3-} vs. sNO_3^-, **(b)** sPO_4^{3-} vs. *s*DIC, and **(c)** sNO_3^- vs. *s*DIC. Observations within the mixed layer (~ depth < 50 m) are illustrated by black circles. The light grey dots in **(b)** and **(c)** show *s*DIC corrected for gas exchange as a function of sPO_4^{3-} and sNO_3^-, respectively. A linear fit is represented by the solid black line for the mixed layer, by the solid grey line for all data, and by the light grey line for the gas-exchange corrected *s*DIC in **(b)** and **(c)**. The dashed black lines are the nutrient drawdown lines using the corresponding Redfield ratio and data from the Upper Circumpolar Deep Water (UCDW) as end-members.

BGD
12, 6929–6969, 2015

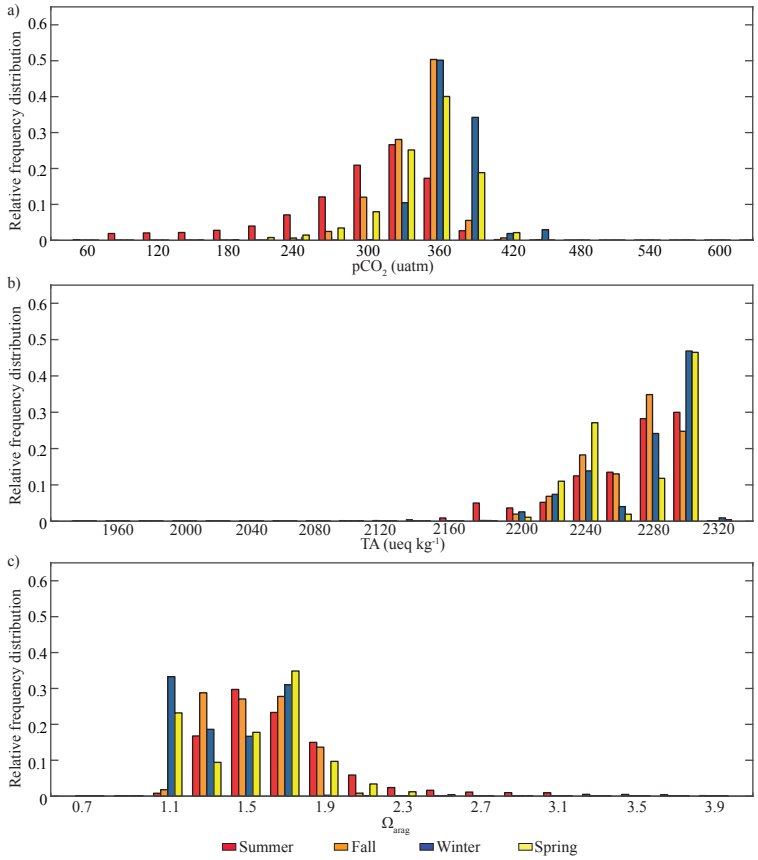

Figure 8. Seasonal variability of inorganic carbon dynamics. Relative frequency distribution of **(a)** measured underway surface partial pressure pCO_2 (uatm), **(b)** predicted surface total alkalinity (TA, ueq kg^{-1}) from underway salinity, and **(c)** predicted surface aragonite saturation state (Ω_{arag}) in summer (red), fall (orange), winter (blue), and spring (yellow). The *x* axis represents the range of Ω_{arag}, TA, and pCO_2 with a relative frequency distribution ≥ 0.0001.

BGD
12, 6929–6969, 2015

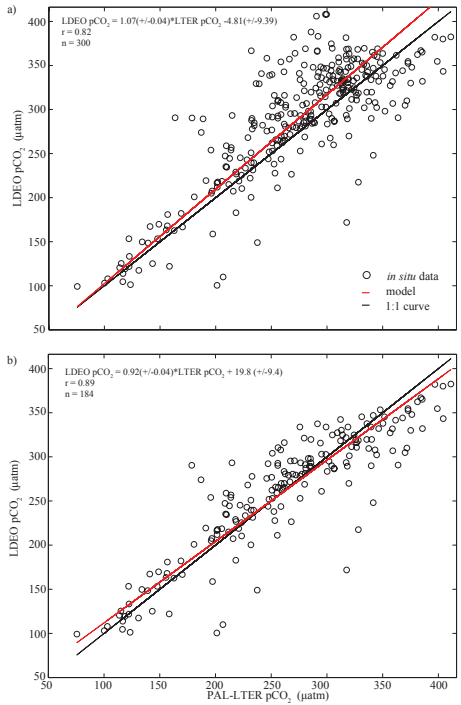

Figure A1. Comparison of Lamont–Doherty Earth Observatory of Columbia University (LDEO) continuous underway pCO_2 (uatm) over the Palmer-Long Term Ecological Research (PAL-LTER) sampling grid (Takahashi et al., 2013) with pCO_2 (uatm) derived from PAL-LTER dissolved inorganic carbon (DIC, umol kg^{-1}) and total alkalinity (TA, ueq kg^{-1}) from discrete samples taken during the same cruise. After clear outliers were removed, the two data sets were spatially matched, with a 1 km distance threshold. **(a)** Years 2002 and 2005–2012, **(b)** Years 2005–2007 and 2011. See Table 1 for statistics.

BGD
12, 6929–6969, 2015

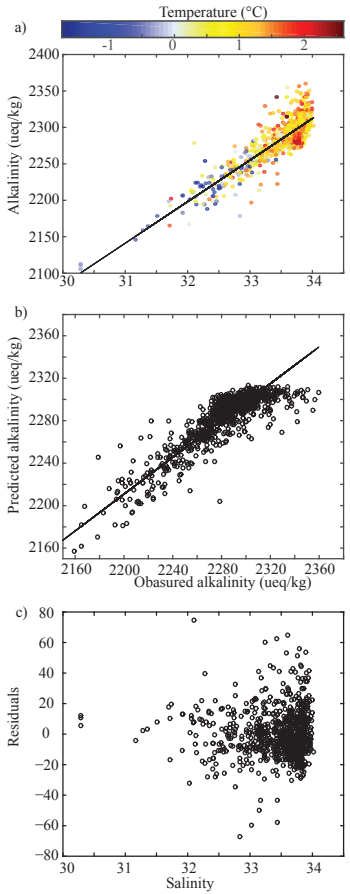

Figure A2. Evaluation of total alkalinity prediction (TA^{pred}) algorithm. **(a)** Measured TA as a function of salinity and temperature (color), **(b)** measured TA vs. TA^{pred}, and **(c)** residuals vs. salinity.

BGD
12, 6929–6969, 2015

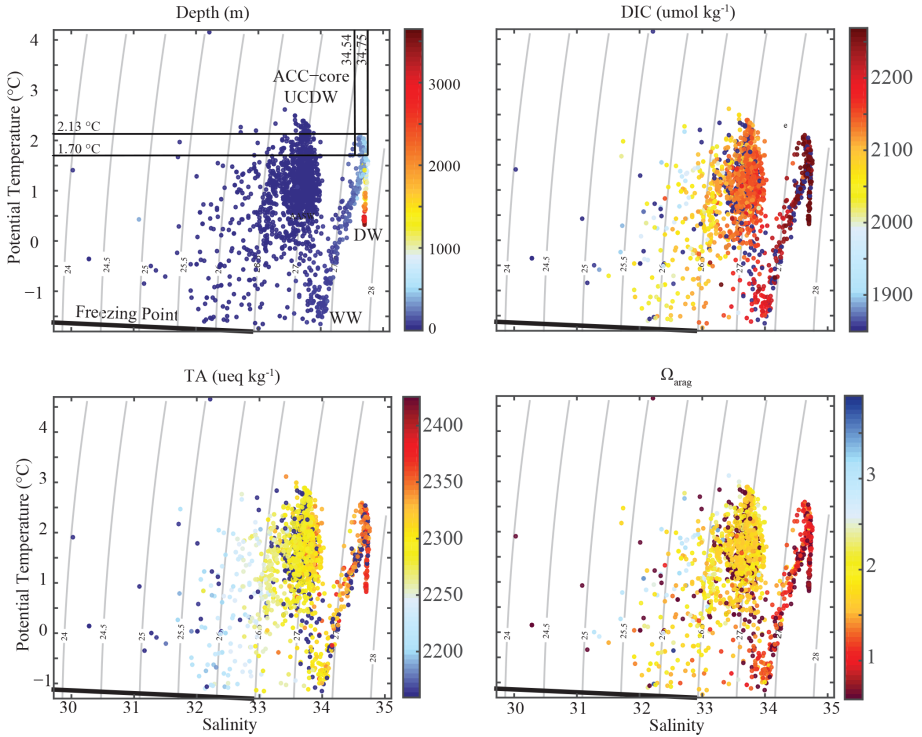

Figure A3. Scatterplots of depth and inorganic carbon chemistry superimposed on potential temperture-salinity diagrams. Shown in color are **(a)** depth, **(b)** dissolved inorganic carbon (DIC, umol kg^{-1}), **(c)** total alkalinity (TA, ueq kg^{-1}), and **(d)** aragonite saturation state (Ω_{arag}). The bold black line illustrates the freezing point as a function of temperature and salinity. Grey lines mark densities. Water masses are indicated and labeled in **(a)**: WW = Winter Water, AASW = Antarctic Surface Water in summer, ACC-core UCDW = Antarctic Circumpolar Current-core Upper Circumpolar Deep Water, DW = local Deep Water end member, following Martinson et al. (2008).

BGD
12, 6929–6969, 2015